ISBN: 978-3-95450-204-2 ISSN: 2673-5350 doi:10.18429/JACoW-IBIC2019-TUPP012

IMAGE OF THE TRANSVERSE BUNCH PROFILE VIA COTR *

A. Potylitsyn†, L. Sukhikh, T. Gusvitskii, Tomsk Polytechnic University (TPU), Tomsk, Russia
G. Kube, A. Novokshonov, Deutsches Elektronen Synchrotron (DESY), Hamburg, Germany

Abstract

The use of Optical Transition Radiation (OTR) monitors is a standard technique to measure transverse beam profiles at many electron accelerators. With modern accelerator technology it is possible to produce and accelerate even ultrashort electron bunches with sub-femtosecond duration. Such bunches interacting with the OTR target generate coherent optical transition radiation (COTR). For the COTR case, a reconstruction of the bunch profile from a recorded image using a conventional optical scheme is a task with inconclusive solution. In this paper we propose an approach which is based on the strict propagation of COTR fields through a focusing lens. As result we obtain a linear dependence of the measured rms image size on the bunch size.

INTRODUCTION

Optical transition radiation (OTR) monitors are widely used for transverse beam profile measurements of accelerated electron beams [1–4]. Such a technique can provide a sub-micron spatial resolution using the so-called "point spread function (PSF) dominated regime" [5]. In a recent publication [6] an approach based on the OTR characteristics using Zemax OpticStudio© [7] was developed which allows to take into account parameters of real optical systems. However, OTR monitors are able to measure only beam profiles for incoherent radiation, i.e. bunch length or bunch sub-structures have to be much longer than the OTR wavelength. Because of modern accelerator technologies as laser-driven plasma accelerators or free electron lasers [8–10] allow to generate sub-femtosecond and even attosecond electron bunches, they demand new diagnostic approaches [11]. Evidently, radiation in the visible spectral region of these bunches becomes coherent such that conventional OTR techniques cannot be applied any more. In this case, the radiation intensity depends on the squared number of electrons in the bunch, and the spectral-angular distribution of coherent OTR (COTR) is determined by the one of conventional incoherent OTR and the bunch form factor [12]. A profile image using COTR and measured with a standard optical system consisting of a focusing lens is a ring structure with a deep central minimum [13]. A few approaches were developed in order to reconstruct COTR generated bunch profiles using a conventional OTR monitor [13–16], but the approximations in use were rough, detailed simulations of this process meet a lot of troubles. In our work we give a consistent description of the optical scheme for COTR allowing to connect image parameters with the bunch size.

* This work was partly supported by the program "Nauka" of the Russian Ministry of Science, grant # 3.1903.2017
† potylitsyn@tpu.ru

MODEL

We consider the standard optical scheme which is illustrated in Fig. 1 together with the coordinate system in use. To simplify the final expressions describing the pattern in the detector plane and taking into account an initial beam profile, following Ref. [17] we use the dimensionless variables

$$\begin{aligned} \{x_T, y_T\} &= \frac{2\pi}{\gamma\lambda}\{X_T, Y_T\} \\ \{x_L, y_L\} &= \frac{\gamma}{a}\{X_L, Y_L\} \\ \{x_D, y_D\} &= \frac{\gamma}{a}\{X_D, Y_D\}, \end{aligned} \tag{1}$$

with γ the Lorentz factor, λ the radiation wavelength, and a the distance between target and lens. Cartesian coordinates indicated by small letters $\{x_i, y_i\}$ are dimensionless ones, by capital letters $\{X_i, Y_i\}$ dimensioned ones, the indices $i = T, L, D$ corresponds to target (T), lens (L) and detector (D) plane.

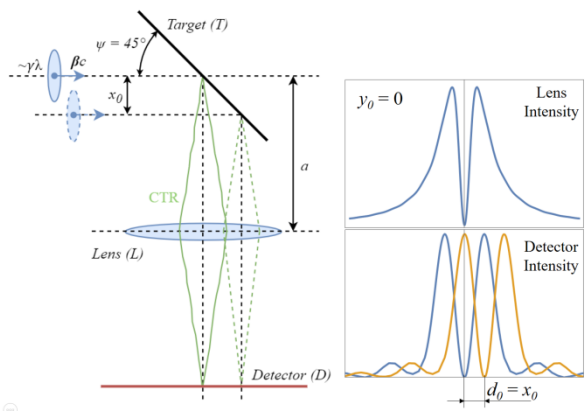

Figure 1: Typical scheme of OTR beam profile monitor.

In the limit of ultra-relativistic electron energies ($\gamma \gg 1$) the OTR process is described as a reflection of the electron field by a perfectly conducting target (an ideal mirror). For a particle passing through an optical system with trajectory coordinates $\{x_0, y_0\}$ relative to the optical axis (impact parameter $\sqrt{x_0^2 + y_0^2}$) it is straightforward to express the fields in the detector plane in paraxial approximation [17]:

$$\begin{aligned} &E^D_{\{x,y\}}(x_D, y_D, x_0, y_0) = \text{const.} \times \\ &\int dx_T\, dy_T \frac{\{x_T - x_0, y_T - y_0\}}{\sqrt{(x_T - x_0)^2 + (y_T - y_0)^2}} \times \\ &\mathrm{K}_1\left(\sqrt{(x_T - x_0)^2 + (y_T - y_0)^2}\right) \exp\left[i\frac{x_T^2 + y_T^2}{4\pi R}\right] \times \\ &4\frac{\sin\left[x_m\left(x_T + \frac{x_D}{M}\right)\right]}{x_T + \frac{x_D}{M}} \times \frac{\sin\left[y_m\left(y_T + \frac{y_D}{M}\right)\right]}{y_T + \frac{y_D}{M}}. \end{aligned} \tag{2}$$

ISBN: 978-3-95450-204-2 ISSN: 2673-5350 doi:10.18429/JACoW-IBIC2019-TUPP012

Here $K_1(t)$ is the modified Bessel function, $R = \frac{a}{\gamma^2\lambda}$, $\{x_m, y_m\}$ the aperture of the square lens, M the optical magnification, dimensioned constants are omitted. The integration in Eq. (2) is performed over the target surface $(-x_{T_{\max}} < x_T < x_{T_{\max}}, -y_{T_{\max}} < y_T < y_{T_{\max}})$.

The OTR pattern in the detector plane (the intensity distribution) from a particle with impact parameter $\{x_0, y_0\}$ is calculated according to

$$\frac{d^2W_0^D{}_{\{x,y\}}}{dx_D, dy_D} = \text{const.} \left| E^D_{\{x,y\}}(x_D, y_D, x_0, y_0) \right|^2 . \quad (3)$$

Figure 2 illustrates the difference between OTR based electron images with $x_0 = 0$ and $x_0 \neq 0$. If $M = 1$ the shift of the OTR intensity minimum is equal to the impact parameter x_0. We used the following parameters for the calculations: $\gamma = 1000$, $\lambda = 0.5$ µm, $a = 500$ mm, $M = 1$, $X_{L_{\max}} = Y_{L_{\max}} = 25$ mm (corresponding to an angular lens aperture of $50\gamma^{-1}$). We would like to emphasize that the pattern shape does not depend on the impact parameter and can be described as

$$\frac{d^2W_0^D{}_{\{x,y\}}}{dx_D, dy_D} = \text{PSF}(x_D - x_0, y_D - y_0) . \quad (4)$$

This fact is used to extract beam sizes from measured patterns if such distribution (the so called Point Spread Function or PSF) is calculated for the parameters before.

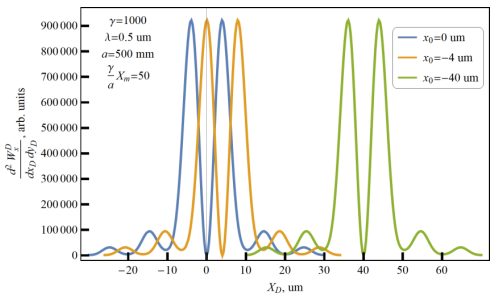

Figure 2: OTR image distributions generated from electrons with different impact parameters.

COTR CASE

According to Eq. (4) the image generation in case of incoherent OTR can be interpreted as PSF convolution with the bunch profile. For COTR it is not the intensity but the particle field which has to be considered. For simplicity the resulting fields for a bunch with Gaussian distribution

$$\rho(x_b, y_b, z_b) = \frac{\exp\left\{-\frac{x_b^2}{2\sigma_x^2} - \frac{y_b^2}{2\sigma_y^2} - \frac{z_b^2}{2\sigma_z^2}\right\}}{(2\pi)^{3/2}\sigma_x\sigma_y\sigma_z} \quad (5)$$

are calculated with σ_x, σ_y, and σ_z the rms bunch sizes. Instead of the two-fold integration in Eq. (2) a five-fold integration (over target surface and bunch volume) has to be performed. The integration over z can be removed if the COTR pattern is measured for a narrow spectral bandwidth $\Delta\lambda/\lambda \ll 1$ because in this case the z-integration is reduced to a multiplication by $\exp\{-4\pi^2\lambda^2/\sigma_z^2\}$. Even after this simplification the remaining integration

$$E^D_{\text{coh}\,\{x,y\}}(x_D, y_D, \sigma_x, \sigma_y) = \text{const} \int \frac{dx_b dy_b}{2\pi\sigma_x\sigma_y} \times \times \exp\left\{-\frac{x_b^2}{2\sigma_x^2} - \frac{y_b^2}{2\sigma_y^2}\right\} E^D_{\{x,y\}}(x_D, y_D, x_b, y_b). \quad (6)$$

requires a large amount of computing power. For further simplification, real and imaginary part of Eq. (6) have been compared. The imaginary part is about a factor 1000 smaller and therefore can be omitted in the intensity calculation.

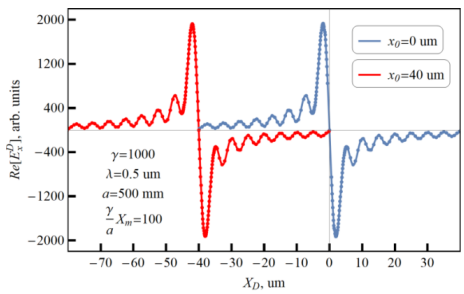

Figure 3: Distribution of OTR fields on the detector plane produced by electrons with different impact parameters.

In Fig. 3 the components $\Re[E_x^D]$ for the impact parameters $x_0 = 0$ and 40 µm are compared. As can be seen the shapes are identical, the only difference is a shift $\Delta x_0 = 40$ µm. This coincidence allows to introduce an "universal" field shape in order to describe the field $\Re[E_x^D]$ for any impact parameter. For further simulations the field was therefore approximated by an analytic expressions with fitted parameters. The field $\Re[E_x^D]$ in Fig. 3, for instance, was fitted by the function

$$E_x^D(x_D) = a_0 x_D \exp\{-b_0 x_D^2\} + \sum_{i=1}^{n} a_k \sin(b_k x_D). \quad (7)$$

The number of terms in this equation is determined by the required accuracy. In the present example the number $n = 10$ was chosen for the a_k coefficients using an angular lens aperture of $50\gamma^{-1}$. The first exponential term in Eq. (7) describes the "long-scale" behaviour of the field, the summation in Eq. (7) is determined by short period oscillations. This expression, which is hereafter called "Field Point Spread Function" (FPSF), allows to calculate the sum of the COTR fields from all electrons in a bunch according to

$$E^D_{\text{coh}\,\{x,y\}}(x_D, y_D, \sigma_x, \sigma_y) = \text{const.} \times \int dx_b dy_b \rho(x_b, y_b) \times \text{FPSF}_{\{x,y\}}(\{x_D - x_b\}, \{y_D - y_b\}) . \quad (8)$$

The easiest way to obtain the 2-dimensional FPSF is to calculate the radial polarization component of the field in

ISBN: 978-3-95450-204-2 ISSN: 2673-5350 doi:10.18429/JACoW-IBIC2019-TUPP012

the far-field zone. In the target size limit $X_{T_{\max}}, Y_{T_{\max}} \to \infty$ it is possible to derive a simple expression for the radial field instead of Eq. (2) (see Ref. [17]):

$$E_r^D(r_D) = \text{const.} \int_0^{r_m} r_L/(1+r_L^2)\mathrm{J}_1(r_L r_D) r_L dr_L, \quad (9)$$

with $r_L = \sqrt{x_L^2 + y_L^2}$, $r_D = \sqrt{x_D^2 + y_D^2}$, $r_m = \sqrt{x_m^2 + y_m^2}$. For the lens aperture $r_m \gg 1$ the field can be presented as follows [18]:

$$E_r^D(r_D) = \text{const.} \left\{ \frac{1}{r_D}[r_D \mathrm{K}_1(r_D) - \mathrm{J}_0(r_D r_m)] \right\}, \quad (10)$$

and consequently,

$$E^D_{\{x,y\}}(x_D, y_D, r_m) = \text{const.} \times \left\{ -\frac{\{x_D, y_D\}}{x_D^2 + y_D^2} \left[\sqrt{x_D^2 + y_D^2}\,\mathrm{K}_1\left(\sqrt{x_D^2 + y_D^2}\right) - \right.\right. \left.\left. -\mathrm{J}_0\left(\sqrt{x_D^2 + y_D^2}\sqrt{x_m^2 + y_m^2}\right)\right]\right\}. \quad (11)$$

The comparison of both fields calculated with Eqs. (2) and (11) are shown in Fig. 4. As can be seen, there is a reasonable agreement between both field descriptions. Therefore in the following the 2-dimensional FPSF is calculated based on the field approximation Eq. (11).

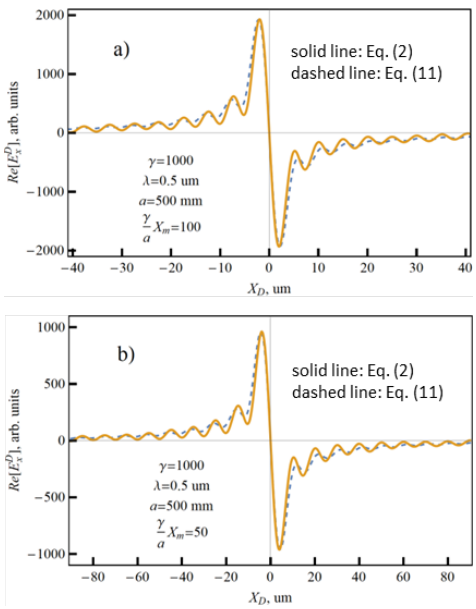

Figure 4: Comparison of the fields calculated using Eqs. (2) and (11) for different lens apertures.

SIMULATION RESULTS

With knowledge of the FPSF it is possible to calculate an image of the bunch profile. Such a calculation should be performed taking into account both contributions from incoherent and coherent OTR fields. Performing the transition from a discrete electron bunch distribution to a continuous one [12], it is possible to derive the expression for both incoherent and coherent OTR intensity distributions in the image plane from a bunch with N particles, introducing a 2-dimensional Gaussian distribution for $\rho(x_b, y_b)$. As a rule, $N \geq 10^6$ and it is sufficient to consider only the COTR contribution. Furthermore, in the following the 1-dimensional dependence of the COTR image on the dimensionless transverse beam size $\sigma_x = \frac{2\pi}{\gamma\lambda}\Sigma_x$ (with Σ_x the rms size in micrometer) will be considered:

$$E^D_{\mathrm{coh}}(x_D, \sigma_x) = \int dx_b \frac{1}{\sqrt{2\pi}\sigma_x} \times \exp\left\{-\frac{x_b^2}{2\sigma_x^2}\right\} E_x^D(x_D - x_b). \quad (12)$$

CHARACTERISTICS OF THE COTR IMAGE

1-dimensional images calculated for a bunch profile and different beam sizes based on Eq. (7) are shown in Fig. 5. As can be seen, the position of the maximum x_m^D in the detector plane depends on the beam size. In Fig. 6 this maximum position as function of the beam size σ_x is shown, having a linear dependency which is described by the linear fit function

$$x_m = 0.034 + 1.14\,\sigma_x\,. \quad (13)$$

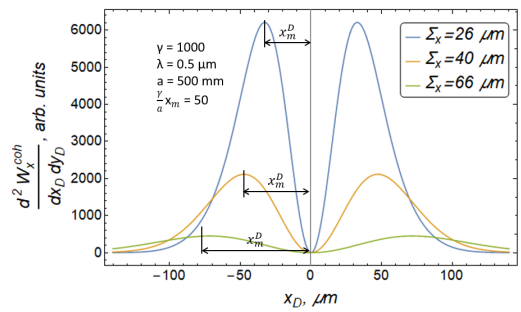

Figure 5: 1-dimensional COTR distributions for different bunch sizes.

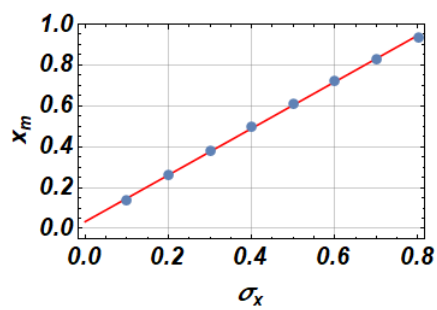

Figure 6: Dependency of the maximums position x_m on the bunch size σ_x.

ISBN: 978-3-95450-204-2 ISSN: 2673-5350 doi:10.18429/JACoW-IBIC2019-TUPP012

It is straightforward to rewrite Eq. (13) in dimensioned units. In principle this equation allows directly to estimate the beam size Σ_x from the maximum X_m of the measured COTR based image.

Hereafter an analogue characteristic for the 2-dimensional case will be deduced. Distributions are calculated along the axes $y_D = 0$ and $x_D = 0$ using the corresponding polarizations, see Eq. (11). For asymmetric bunches these distributions should be distinguished. Such difference can be

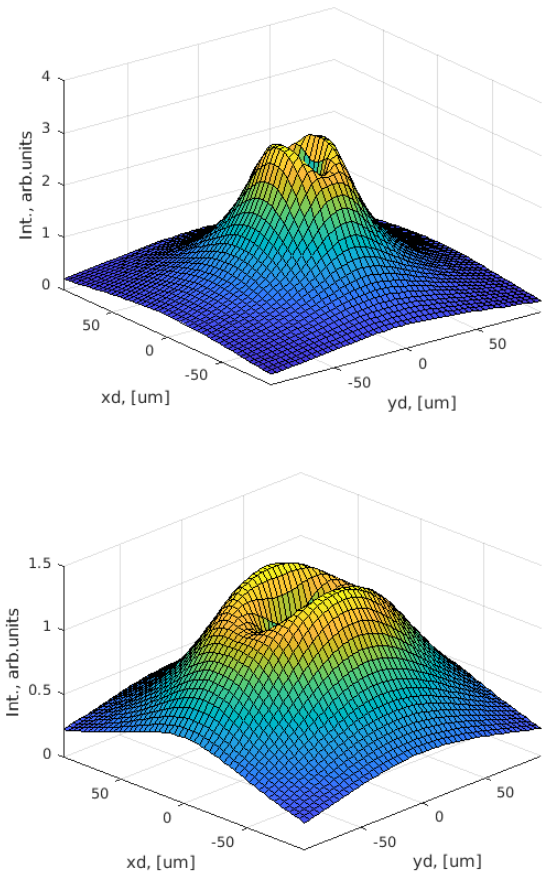

Figure 7: 2-dimensional COTR distributions, calculated for $\gamma = 1000$ and $\lambda = 0.5$ µm. Top: $\Sigma_x = 16$ µm, $\Sigma_y = 8$ µm; bottom: $\Sigma_x = 16$ µm, $\Sigma_y = 32$ µm.

observed in Fig. 7 (top: $\sigma_x = 0.2$, $\sigma_y = 0.1$, and bottom: $\sigma_x = 0.2$, $\sigma_y = 0.4$). The 1-dimensional distributions for the latter case are presented in Fig. 8. It should be noted that Eq. (13) is valid only for the distribution along the major axis of the bunch profile, i.e. the condition $\sigma_x^2 \gg \sigma_y^2$ has to be fulfilled. For a round bunch ($\sigma_x = \sigma_y$) the distribution along y_D (or x_D) may be considered as radial distribution of the image. For such azimuthal symmetric bunch the position of the maximum is described by a linear dependence with an increased coefficient compared to the case under consideration in Eq. (13) : $r_m = 0.027 + 1.36\,\sigma$.

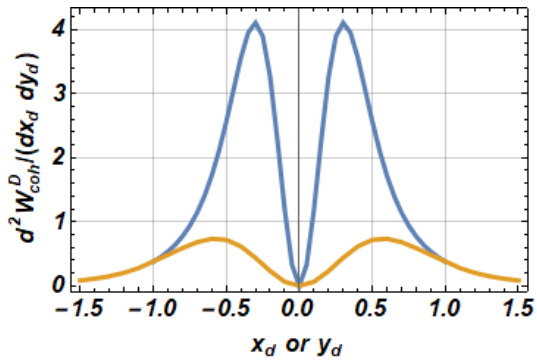

Figure 8: 1-dimensional distributions $d^2W^D_{\rm coh}/(dx_d dy_d)$ for the case $\sigma_x = 0.2$ and $\sigma_y = 0.4$. Blue curve: $y_d = 0$, yellow curve: $x_d = 0$.

DISCUSSION AND CONCLUSION

The authors of Ref. [15] proposed to describe the COTR profile in the image plane by the expression

$$I_{\rm coh} \sim |\delta_x \rho_\perp(x_D, y_D)|^2 + |\delta_y \rho_\perp(x_d, y_D)|^2. \qquad (14)$$

For a Gaussian bunch profile, the image will therefore be described again by a Gaussian

$$I_{\rm coh} \sim \left(\frac{x_D^2}{\sigma_x^4} + \frac{y_D^2}{\sigma_y^4}\right) \exp\left\{-\frac{x_D^2}{\sigma_x^2}\right\} \exp\left\{-\frac{y_D^2}{\sigma_y^2}\right\}. \qquad (15)$$

For a round bunch this distribution posses a maximum at $r_d = \sigma$ which is smaller than the simulation result of the present work (rms about $1.36\,\sigma$). On the other hand the author of Ref. [19] simulated an image for a round bunch and obtained an intensity distribution in the image plane with the maximum at $r \approx 1.6\,\sigma$ which is close to our calculations.

The approach presented in this work allows to perform a quantitative analysis of bunch profiles measured with COTR and a focusing lens. Expressions were obtained for both polarization components E_x, E_y of the COTR field. In the model, a finite area of the OTR target and a finite lens aperture were taken into account.

The propagation of COTR through an optical system was simulated as convolution of the COTR field in the image plane with a distribution describing the transverse bunch profile (in contrast to incoherent OTR where such convolution is performed with the intensity but not with the field). For a bunch with Gaussian transverse beam profile, images were calculated assuming a conventional optical system. It was shown that the resulting distributions are characterized by a central minimum along the beam direction, and that the position of the intensity maxima is determined by the transverse bunch size.

In the experiment described in Ref. [20] the authors observed COTR interference fringes from an ultra-relativistic electron bunch ($E = 215$ MeV) using two OTR screens. Such a bunch generated by the mechanism of laser-plasma acceleration possesses a strong asymmetry in the $x - y$ plane. The approach described above can be applied for simulation of COTR characteristics from such kind of bunches.

ISBN: 978-3-95450-204-2 ISSN: 2673-5350 doi:10.18429/JACoW-IBIC2019-TUPP012

REFERENCES

[1] X. Artru, R. Chehab, et al., "Resolution power of optical transition radiation. Theoretical considerations", *Nucl. Instrum. Methods in Phys. Res. B*, vol. 145 (1-2), pp. 160–168 (1998).

[2] A.H. Lumpkin, B.X. Yang, et al., "Optical techniques for electron-beam characterizations on the APS SASE FEL project", *Nucl. Instrum. Methods in Phys. Res. A*, vol. 429, pp. 336–340 (1999).

[3] M. Ross, S. Andersen, et al., "A very high resolution optical transition radiation beam profile monitor", SLAC-PUB-9280 (2002).

[4] A. Cianchi, M. Castellano, et al., "Nonintercepting electron beam size monitor using optical diffraction radiation interference", *Phys. Rev. ST-AB*, vol. 14, p. 102803 (2011).

[5] P. Karataev, A. Aryshev, et al., "First Observation of the Point Spread Function of Optical Transition Radiation", *Phys. Rev. Lett.*, vol. 107, p. 174801 (2011).

[6] J. Wolfenden, R.B. Fiorito and C.P. Welsch, "A novel simulation and analysics algorithm for high resolution optical transition radiation imaging", *Opt. Express*, vol. 27(3), p. 2988 (2019).

[7] Zemax Optic Studio 16.5, User's Manual, Zemax, 2017.

[8] W. P. Leemans, C. G. R. Geddes, et al., "Observation of Terahertz Emission from a Laser-Plasma Accelerated Electron Bunch Crossing a Plasma-Vacuum Boundary", *Phys. Rev. Lett.*, vol. 91, p. 074802 (2003).

[9] E. Saldin, E. Schneidmiller, M. Yurkov, "The Physics of Free Electron Lasers", Springer-Verlag, 2010.

[10] U. Dorda, R. Assmann, et al, "SINBAD - The accelerator R& D facility under construction at DESY", *Nuclear Instruments and Methods in Physics Research A*, vol. 829, pp. 233-236 (2016).

[11] M. C. Downer, R. Zgadzaj, et al., "Diagnostics for plasma-based electron accelerators", *Rev. of Mod. Phys.*, vol. 90, p. 035002 (2018).

[12] C. B. Schroeder, E. Esarey, et al., "Theory of coherent transition radiation generated at a plasma-vacuum interface", *Phys. Rev. E*, vol. 69, p. 016501 (2004).

[13] H. Loos, R. Akre, et al., "Observation of coherent optical transition radiation in the LCLS Linac", SLAC-PUB-13395 (2008).

[14] R. B. Fiorito *et al.*, "Simulation of Coherent Optical Transition Radiation in Linac Based Free Electron Lasers", in *Proc. 31st Int. Free Electron Laser Conf. (FEL'09)*, Liverpool, UK, Aug. 2009, paper TUPC49, pp. 356–359.

[15] N. Bourgeois, M. Heigoldt, et al, "Transverse beam profile measurements of laser accelerated electrons using coherent optical radiation", *Proc. AIP Conf.*, vol. 1507, p. 258 (2012).

[16] G. Geloni, P. Ilinski, E. Saldin, E. Schneidmiller, and M. V. Yurkov, "Coherent Optical Transition Radiation as a Tool for Ultra-Short Electron Bunch Diagnostics", in *Proc. 9th European Workshop on Beam Diagnostics and Instrumentation for Particle Accelerators (DIPAC'09)*, Basel, Switzerland, May 2009, paper TUPB37, pp. 251–253.

[17] A.P. Potylitsyn. "Advanced Radiation Sources and Applications", *NATO Science Series II*, Springer, N.Y., 199, 149 (2006).

[18] Dao Xiang, Wen-Hui Huang, and Yu-Zheng Lui, "Imaging of high-energy electron beam profile with optical diffraction radiation", *Physical Review Special Topics – Accelerators and Beam*, vol. 10, p. 062801 (2007).

[19] G. Stupakov, "Image formation by incoherent and coherent transition radiation from flat and rough surfaces", SLAC-PUB (2011).

[20] A. Lumpkin, M. LaBerge, et al., "Observations of Coherent Optical Transition Radiation Interference Fringes Generated by Laser Plasma Accelerator Electron Beamlets", FERMILAB-CONF-18-511-AD, (2018).